Twin-image problem in digital holography—a survey

(Invited Paper)

Elena Stoykova[1,2], Hoonjong Kang[1*], and Jiyung Park[1]

[1] *Realistic Media Platform Center, Korea Electronics Institute of Technology, 8 Floor, #1599 Sangam-dong, Mapo-gu, Seoul 121-835, Korea*

[2] *Permanently with Institute of Optical Materials and Technologies, Bulgarian Academy of Sciences, Acad. G. Bonchev, Str. 109, 1113 Sofia, Bulgaria*

[*] *Corresponding author: hoonjongkang@keti.re.kr*

Received January 29, 2014; accepted April 4, 2014; posted online May 20, 2014

Zero-order and twin images are a serious obstacle in achieving a high-quality output in in-line digital holography (DH). They decrease the useful bandwidth of the off-axis DH. Over the years the twin image removal problem was approached both by instrumental and numerical means. The paper provides an extended survey of the proposed solutions with their pros and cons as a guide for further advance in this field. Processing of a single spatial carrier fringe pattern involves spatial filtering in the frequency domain, spatial phase-shifting (PS) or wavelet transform. A point source digital holographic microscopy (DHM), introduction of calibration measurements or various modifications of PS technique are instrumental solutions to the twin image problem for in-line DH. Numerical solutions to the same problem include iterative and non-iterative approaches, diffraction-based and inverse problem solutions, reconstruction of purely real or phase objects and of complex objects, reconstruction of plane and volume objects. Elimination only of the zero-order image relies on non-linear filtering or additional calibration measurements.

OCIS codes: 090.0090, 090.1995, 100.3010.

doi: 10.3788/COL201412.060013.

1. Introduction

Holography is a two-step process which enables storing and reconstruction of a wave field diffracted by three-dimensional (3D) objects. The hologram records as a two-dimensional (2D) intensity pattern the interference of this wave field with a mutually coherent reference wave. By coding the phase of the diffracted field through a non-linear detection process in a real-valued fringe pattern, the hologram yields in reconstruction two beams with the same information content. They focus on the opposite sides of the hologram forming the so called twin images. In addition, a much brighter zero-order image is produced by the non-informative slowly varying background intensity in the hologram. In in-line holography, first introduced by Dennis Gabor[1] in 1948 by proposing a point source illumination of a semi-transparent object, the beams forming the zero-order and twin images overlapped in space. Leith and Upatnieks[2] separated these beams in the off-axis holography in 1962 through introduction of a spatial carrier frequency in the hologram. Rapid progress in digital megapixel photosensors (CCDs or CMOS sensors) and computers two decades later turned a purely academic idea of digital holography (DH), advanced in the early 1970s, into a powerful tool in optical metrology[3,4]. The hologram is sampled and digitized by the image photo-sensor, stored in the computer and numerically reconstructed[5,6]. Thus numerical focusing at a variable depth of 3D objects, capture of both amplitude and phase information and hence observation of transparent micro-objects without labeling and stimulating agents, determination of size, localization and tracking of particles in a 3D volume became feasible.

The in-line DH with its simple set-up without additional lenses, beam-splitters and mirrors has proved its potential for fluid-flow imaging[7,8], study of particles and aerosols[9], phase-contrast imaging in a soft X-ray microscopy with a high signal-to-noise ratio[10], gamma-ray holography[11] and photoelectron emission holography[12]. However, both zero-order and twin images are a serious obstacle in achieving a high-quality output of the measurement. These parasitic images decrease the useful bandwidth and deteriorate also the output of the off-axis DH.

Over the years the twin image removal problem was approached both by instrumental and numerical means. The goal of this paper is to provide an extended survey of the proposed solutions with their pros and cons as a guide for further advance in this field. The structure of the paper is as follows: after giving a brief theoretical background in Section 2, we first discuss spatial carrier-frequency approaches in Section 3. Sections 4 and 5 focus on in-line holography by dividing the existing methods into instrumental and numerical solutions respectively. Description of solutions for elimination of the zero-order image only is given in Section 6.

2. Theoretical background

Figure 1 depicts schematically the two-step process of holographic recording and reconstruction. Interference of the object wave field with a complex amplitude, $O(x,y) = a_{\mathrm{O}}(x,y)\exp[i\varphi_{\mathrm{O}}(x,y)]$, which carries information about the object, and the mutually coherent reference field, $R(x,y) = a_{\mathrm{R}}(x,y)\exp[i\varphi_{\mathrm{R}}(x,y)]$ (Fig. 1(a)), results in four terms superimposed in the hologram plane (x,y)

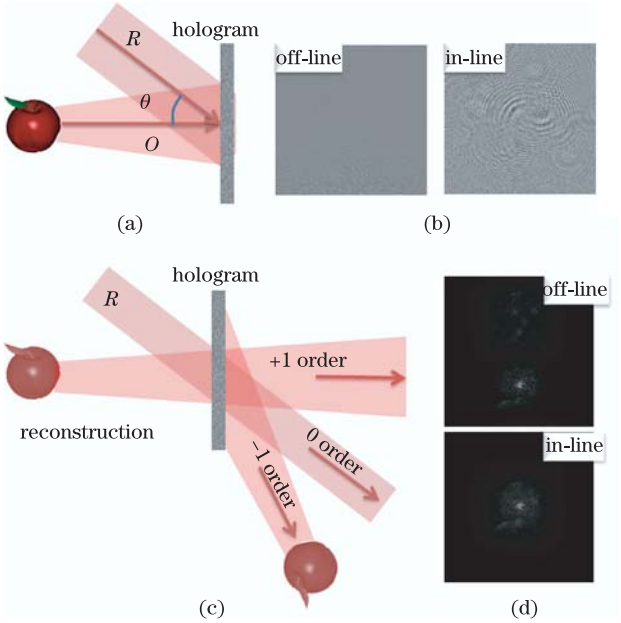

Fig. 1. (Color online) (a) Recording of a hologram; O-object beam, R-reference beam. (b) Off-line ($\theta \neq 0$) and in-line ($\theta = 0$) holograms of an object "apple" calculated by the RS algorithm; the zero order term is omitted. (c) Reconstruction at illumination with the reference wave. (d) Reconstructed images from off-line and in-line holograms in (b).

$$I_{\mathrm{H}}(x,y) = |\boldsymbol{R}(x,y) + \boldsymbol{O}(x,y)|^2 = \boldsymbol{R}\boldsymbol{R}^* + \boldsymbol{O}\boldsymbol{O}^* + \boldsymbol{O}\boldsymbol{R}^* + \boldsymbol{O}^*\boldsymbol{R}, \quad (1)$$

where the asterisk denotes a complex conjugate operator (Fig. 1(b)). The first and the second terms are the intensities of the reference and object waves that form the zero-order term. The last two terms represent +1 and –1 diffraction orders which encode the relevant information. As a rule, the zero-order is much brighter than the first-order terms, and their visualization requires contrast enhancement. Multiplication of $I_{\mathrm{H}}(x,y)$ in DH with the replica of $\boldsymbol{R}(x,y)$ or its conjugate reconstructs the object field $\boldsymbol{O}\boldsymbol{R}^*\boldsymbol{R} = \boldsymbol{O}$ or $\boldsymbol{O}^*\boldsymbol{R}^*\boldsymbol{R} = \boldsymbol{O}^*$, and brings into focus the virtual or the real image (Fig. 1(c)). A plane wave, $\boldsymbol{R}(x,y)$, in acquisition and reconstruction produces non-distorted virtual and real images. The twin images are separated for the off-axis geometry for which the light beams $R(x,y)$ and $O(x,y)$ subtend an angle θ, and they overlap at $\theta = 0$ (Fig. 1(d)). The shown reconstructions correspond to the holograms in Fig. 1(b) that have been calculated from a point-cloud of an apple model using Rayleigh-Sommerfeld (RS) diffraction formula as $\tilde{I}_{\mathrm{H}}(x,y) = 2\Re\{\boldsymbol{O}(x,y)\,\boldsymbol{R}^*(x,y)\}$, where $\boldsymbol{R}(x,y)$ is a plane wave, $\boldsymbol{O}(x,y) = \sum_{p=1}^{P} A_p r_p^{-1} \exp(jkr_p)$, (x_p, y_p, z_p) are the Cartesian coordinates of the object's point, $A_p = a_p \exp(j\phi_p)$ with a_p and ϕ_p being the amplitude and the phase of the light field emanated by this point, and $r_p = \sqrt{(x-x_p)^2 + (y-y_p)^2 + z_p^2}$ is the distance between this point and the point on the hologram; $k = 2\pi/\lambda$ is a wave number, λ is the wavelength, and P is the number of points.

Most of the algorithms in DH simulate propagation of the complex wave $I_{\mathrm{H}}\boldsymbol{R}$ to reconstruct the desired image of the object by applying the scalar diffraction theory[3,13–16]. The Huygens convolution approach reconstructs the complex amplitude, $\Gamma(\xi,\eta,z)$, by solving the integral

$$\Gamma(\xi,\eta;z) = -\frac{j}{\lambda z}\iint_{\Sigma} I'_{\mathrm{H}}(x,y) \cdot \exp\left\{jk\sqrt{(x-\xi)^2 + (y-\eta)^2 + z^2}\right\}\mathrm{d}x\mathrm{d}y, \quad (2)$$

at a distance z from the hologram, where $I'_{\mathrm{H}}(x,y) = I_{\mathrm{H}}(x,y)\,\boldsymbol{R}(x,y)$ and $\sum$ is the 2D aperture of the hologram, as a convolution

$$\Gamma(\xi,\eta;z) = I'_{\mathrm{H}}(x,y) * h(x,y,z) = F^{-1}\{F[I'_H(x,y)]\,F[h(x,y,z)]\}. \quad (3)$$

In Eq. (3), $h(x,y,z) = -\frac{i}{\lambda z}\exp\left\{\mathrm{j}k\sqrt{x^2+y^2+z^2}\right\}$ is the coherent point spread function of the free space propagation[16]and F is a 2D Fourier transform which is given by $G(\nu_x,\nu_y) = F[g(x,y)] = \int_{-\infty}^{\infty}\int_{-\infty}^{\infty} g(x,y)\exp[-\mathrm{j}2\pi(\nu_x x + \nu_y y)]\mathrm{d}x\mathrm{d}y$, where g is a function in the spatial domain and G is its spectrum in the frequency domain. In paraxial approximation the parabolic wave-fronts replace the spherical ones to speed calculation, and the 2D Fresnel convolution kernel

$$h_z(x,y) = \frac{\exp(ikz)}{i\lambda z}\exp\left[\frac{ik}{2z}\left(x^2+y^2\right)\right], \quad (4)$$

is used for propagating the object field to the plane z. The Fresnel kernel has the properties

$$h_z^*(x,y) = h_{-z}(x,y) \quad \text{and} \quad h_{z_1}(x,y) * h_{z_2}(x,y) = h_{z_1+z_2}(x,y). \quad (5)$$

The complex amplitude of the reconstructed field is given by

$$\Gamma(\xi,\eta;z) = 2\pi\exp\left[\frac{jk}{2z}\left(\xi^2+\eta^2\right)\right]F\{I'_{\mathrm{H}}(x,y)\,h_z(x,y)\}. \quad (6)$$

Propagation of spherical waves in Eq. (2) and parabolic waves in Eq. (6) sets limitation on the minimal possible distance between the hologram and the reconstruction plane. Sampling of the wavefront remains equal to that in the hologram plane for the Huygens convolution approach whereas it increases linearly with the distance for the Fresnel approach. A detailed analysis of the spatial resolution in the reconstruction plane for the digital Fresnel holography is made in Ref. [17]. The angular spectrum method, based on propagation of plane waves, also ensures invariable wavefront sampling without any limitations on the reconstruction distance. The complex amplitude of the reconstructed field is found from

$$\Gamma(\xi,\eta;z) = F^{-1}\left\{F[I'_{\mathrm{H}}(x,y)]\exp\left[ik\sqrt{k^2-k_x^2-k_y^2}\right]\right\}, \quad (7)$$

where $\vec{k} = (k_x, k_y, k_z)$ is the wave vector of the propagating wave, and $k_z = \sqrt{k^2 - k_x^2 - k_y^2}$.

Another hologram model for in-line geometry proved to be very useful for digital processing of the holograms. If an object with an opacity function τ imparts a phase shift φ to an illuminating plane wave with a unity amplitude, the beam behind the object is a coherent sum, $(1-\tau)\, e^{i\varphi} = 1 - \vartheta$, of the incident plane wave and the beam interacted with the object. The hologram recorded at distance z from the object is modeled as

$$I_{\mathrm{H}} = 1 - \vartheta * h_z - \vartheta^* * h_z^* - |\vartheta * h_z|^2 \approx 1 - \vartheta * h_z - \vartheta^* * h_{-z}, \tag{8}$$

and its reconstruction at distance z under illumination with the same plane wave is given by

$$\Gamma = 1 - \vartheta^* - \vartheta * h_{2z}. \tag{9}$$

The contribution of the so called intermodulation term, $\boldsymbol{OO}^*$, is neglected in Eqs. (8) and (9). The diffraction based reconstruction methods mimic the physical process of optical reconstruction which leads inevitably to the presence of the zero-order image and the out-of-focus twin-image in the observation plane. They do not solve the inverse problem[18,19] because the output,

$$\Gamma(\xi, \eta) = \delta(\xi, \eta) + 2Re\left[h_{2z}(\xi, \eta)\right], \tag{10}$$

after the reconstruction of a hologram of a point object, $I_{\mathrm{H}} \propto 1 - h_z - h_{-z}$, is not a point in the observation plane. Actually, the second term in Eq. (9) is the diffraction pattern of a point object located at a distance $2z$ from the observation plane.

3. Spatial carried-frequency approaches

The spectrum of the hologram in the spatial frequency domain (ν_x, ν_y) is given by

$$\begin{aligned} W(\nu_x, \nu_y) =& F\left\{\boldsymbol{RR}^* + \boldsymbol{OO}^* + \boldsymbol{OR}^* + \boldsymbol{O}^*\boldsymbol{R}\right\} \\ =& W_{\mathrm{R}}^0 + W_{\mathrm{O}}^0 + W_{\mathrm{v}}^1 + W_{\mathrm{r}}^1, \end{aligned} \tag{11}$$

where $W_{\mathrm{R,O}}^0$ are the spectra of the reference and object beams intensities while $W_{\mathrm{v,r}}^1$ give the spectra of the virtual and real image terms. The terms W_{O}^0 and W_{R}^0 are located around the zero frequency in the Fourier domain. If the object spectrum is confined within an area $B_\nu \times B_\mu$, W_{O}^0 covers an area of $2B_\nu \times 2B_\mu$. The spread of the spectrum W_{R}^0 depends on the hologram aperture. For a plane reference wave and an infinite hologram, W_{R}^0 is a delta-function.

Introduction of a spatial carrier frequency by tilting the reference beam at an angle θ with respect to the hologram-to-object observation axis (Fig. 1(a)), separates spatially $W_{\mathrm{R,O}}^0$ from W_{v}^1 and W_{r}^1. For a plane reference wave $\boldsymbol{R}(x, y) = \exp j\left(k_{\mathrm{R}x}x + k_{\mathrm{R}y}y\right)$, W_{v}^1 and W_{r}^1 are located at $(2\pi)^{-1}(k_{\mathrm{R}x}, k_{\mathrm{R}x})$ and $(2\pi)^{-1}(-k_{\mathrm{R}x}, -k_{\mathrm{R}x})$ in the frequency domain. Requirements to be set upon $k_{Rx}, k_{\mathrm{R}y}$ for optimal separation of the zero and ± 1 orders in the frequency domain for Fresnel DH are formulated in Ref. [17]. By using a window function, $\Omega(\nu_x, \nu_y)$, in the frequency domain, the one of the spectra $W_{\mathrm{v,r}}^1$ is filtered out allowing for reconstruction of the object beam from $O(x, y) = R^*(x, y)\, F^{-1}\left\{F\left[I_{\mathrm{H}}(x, y)\right]\Omega(\nu_x, \nu_y)\right\}$[20]. Effective suppression of the unwanted terms is possible if the angle $\theta = \arcsin\left(\lambda\sqrt{k_{\mathrm{R}x}^2 + k_{\mathrm{R}y}^2}\right)$ separates completely $W_{\mathrm{R,O}}^0$ from $W_{\mathrm{v,r}}^1$. Spatial filtering in the frequency domain (ν_x, ν_y) of one of the diffraction orders by using the window function $\Omega(\nu_x, \nu_y)$ is illustrated in Fig. 2(a). Figure 2(b) presents reconstruction of the off-line hologram without (top) and with (bottom) spatial filtering. The hologram was calculated from a point-cloud of the logo "KETI" using RS diffraction formula.

This approach makes possible real-time operation by using a single hologram for object reconstruction. However, it puts higher demand on the space-bandwidth product of the hologram. This is not a problem in the off-axis analog holography due to the fine structure of the used light-sensitive materials. In the off-axis DH the large size of the pixel pitch, Δp, of the used image photo sensor entails off-axis recording only of small objects at large distances because of the limitation on the maximum angle between the interfering waves that is given by $\theta_{\max} = \arcsin(0.5\lambda/\Delta p)$ for plane waves. The need of a larger space-bandwidth product inevitably worsens spatial resolution of the off-axis DH. A sensor at a distance D from the one-dimensional (1D) object with size L_{O} and bandwidth B should provide a space-bandwidth product $L_{\mathrm{O}}B(1 + \lambda DB/L_{\mathrm{O}})$ for in-line geometry and $4L_{\mathrm{O}}B(1 + \lambda DB/L_{\mathrm{O}})$ for off-axis geometry[15]. Despite this technical drawback, the off-axis DH has established itself as a standard technique for microscopic amplitude and phase-contrast imaging[21,22], including tomographic and polarization imaging[23,24], holographic particle analysis[25], synthetic aperture and low coherence imaging[26,27]. The resolution is improved by a microscopic lens. An off-axis set-up with a low spatial frequency holographic diffraction grating as a beam splitter is presented in Ref. [28].

The spatial filtering approach has such shortcomings as loss of high-frequency components, interference from the other terms in the hologram, need to design a proper

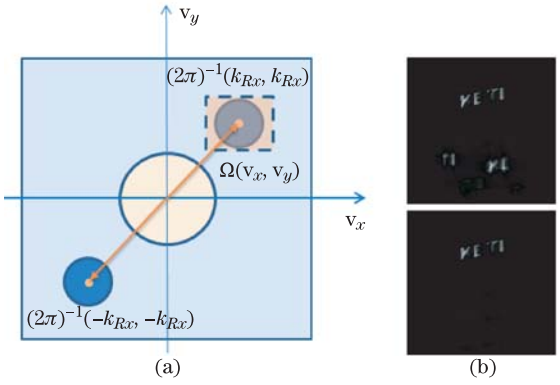

Fig. 2. (Color online) (a) Spatial filtering in the frequency domain (ν_x, ν_y) of one of the diffraction orders by using the window function $\Omega(\nu_x, \nu_y)$. (b) Reconstruction of the off-line hologram of the logo "KETI" without (top) and with (bottom) spatial filtering.

window function, $\Omega(\nu_x, \nu_y)$, edge effects due to the finite size of the hologram, and very often necessity of manual intervention[29]. These drawbacks provoked development of alternative methods for object beam retrieval from a single spatial carrier-frequency hologram. Thus, the DH adopted the spatial carrier phase-shifting (PS) method which is well known in interferometry[30−32]. The unknown object wavefront is derived from a set of phase-shifted intensity values taken from the neighboring pixels to the pixel of interest. It yields reconstruction free of the zero-order and the twin-image. Data are processed in the spatial domain. The algorithm is based on the assumption that the phase to be retrieved, $\varphi_{\mathrm{O}}(x, y)$, varies slowly in comparison to the carrier phase, $\varphi_{\mathrm{R}}(x, y)$, and remains constant in the pixels which give the set of phase-shifted intensities. The phase gradient calculated for the neighboring pixels is accepted equal to the carrier frequency. A plane reference wave should subtend an angle $\sin^{-1}(\lambda/3\Delta p)$ or $\sin^{-1}(\lambda/4\Delta p)$ with the optical axis to apply 3- or 4-step PS algorithm with a phase step $2\pi/3$ or $\pi/2$ respectively. The assumption of a constant phase difference between the pixels introduces a wavefront and algorithm dependent error and limits the abruptness of variation of $\varphi_{\mathrm{O}}(x, y)$. The error decreases if the phase is retrieved from pixels grouped around a given point in two dimensions; in this case a pixelated spatial carrier is introduced by a pixelated phase mask[33,34]. A generalized error formula for n-step PS algorithm applied to a pixelated spatial carrier fringe pattern is derived in Ref. [35]. The phase-shift error is corrected by filtering the spectrum of the one of the twin image terms in Ref. [36].

Reconstruction in off-axis geometry without imitating the diffraction process is proposed in Ref. [37]. The algorithm also resembles the PS approach. The complex amplitude $\boldsymbol{O}(x, y)$ is retrieved in the hologram plane and back-propagated to the object plane. The algorithm relies on a parametric mathematical model of the phase-difference between $\boldsymbol{O}(x, y)$ and $R(x, y)$. The phase of the reference wave, $\varphi_{\mathrm{R}}(x, y)$, and hence the intensity in the hologram plane, I_{H}, vary rapidly in comparison to the quantities, $a_{\mathrm{R}}, a_{\mathrm{O}}, \varphi_{\mathrm{O}}$. Actually, they are assumed constant in the vicinity of a given point. This permits to construct a set of M non-linear equations using the intensity data in M surrounding pixels. This set of equations is solved in the least-squares sense. By introduction of unique auxiliary variables at $a_{\mathrm{R}} > a_{\mathrm{O}}$, the non-linear task for determination of $\boldsymbol{O}(x, y)$ is solved by linear methods. Specially designed weighting functions make the method applicable to a non-planar reference wave. The optimal processing window should cover one period of the interference pattern. A smaller window size produces noise in the reconstructed image. Increasing the window increases the computation time and worsens the spatial resolution. The algorithm complexity is $\mathrm{O}(MN)$, where N is the number of points in the hologram. The algorithm makes use of all pixels in the hologram, provides a larger field of view and a result free of artifacts because no fast Fourier transform is used. An automated method is invented in Refs. [38,39] to obtain the parameters of the phase difference model.

Phase retrieval from a spatial carrier fringe patterns using wavelets has been examined both for profilometry and DH[40−42]. The zero-order and twin image terms are removed by means of a Gabor wavelet[42] which in 1D case is represented by $\psi_{a,b}(\zeta) = \sqrt[-4]{\pi}\sqrt{\alpha}\exp\left[-\alpha^2\zeta^2/2 + j2\pi\zeta\right]$ with $\zeta = (x-b)/a$ and $\alpha = \sqrt{2\ln 2}$. At slow variation of the amplitudes, a_{R}, a_{O}, and the gradient of the object phase, the wavelet coefficients on the ridge, where the modulus of the transform is maximum, are proportional to $\boldsymbol{O}(x, y)$ multiplied by a constant. The technique allows for reconstruction of dynamic objects because no spatial filtering is required.

Table 1 summarizes the main properties of the spatial-carrier frequency solutions for the twin image removal. As it can be seen, the twin image removal is complete at the expense of decreased bandwidth and spatial resolution in comparison with the in-line set-ups. The spatial filtering in the frequency domain as well as the non-linear retrieval of the object wave are the most widely used, e.g., in DHM.

4. In-line geometry—elimination by instrumental means

Simplicity of the in-line holography, in which the object and reference beams are the diffracted and non-diffracted parts of the same beam, its higher resolution and a wide scope of applications inspired search of solutions to cope with the twin-image problem by instrumental means. Implementation of the Gabor original recording scheme (Fig. 3) has been reported for the so-called point-source digital holographic microscopy (DHM)[43,44]. A spherical reference wave $R(\vec{r}, t) = a_{\mathrm{R}}\exp(ikr)/r$, created by a pinhole of about 1-μm size at the origin of the coordinate system, illuminates a small object located at some distance from the pinhole to block a small part of the reference light. A photo sensor at distance L from the pinhole captures the whole light from the pinhole. The object field is determined by using the Kirchhoff-Helmholtz transform

$$\boldsymbol{O}(\vec{\boldsymbol{\xi}}) = -\frac{j}{2\lambda}\int\limits_{\text{screen}} \tilde{I}_{\mathrm{H}}(\vec{r})\,\frac{1}{r^2}\left(1+\frac{r}{L}\right)\exp[ik\vec{\boldsymbol{\xi}}\cdot\vec{\boldsymbol{r}}/r]\boldsymbol{d}^2\vec{\boldsymbol{r}}, \tag{12}$$

where

$$\begin{aligned}\widetilde{I}_{\mathrm{H}}(\vec{\boldsymbol{r}}, t) &= |\boldsymbol{R}(\vec{\boldsymbol{r}}, t) + \boldsymbol{O}(\vec{\boldsymbol{r}}, t)|^2 - |\boldsymbol{R}(\vec{\boldsymbol{r}}, t)|^2 \\ &= [\boldsymbol{R}^*(\vec{\boldsymbol{r}}, t)\,\boldsymbol{O}(\vec{\boldsymbol{r}}, t) + \boldsymbol{R}(\vec{\boldsymbol{r}}, t)\,\boldsymbol{O}^*(\vec{r}, t)] + |\boldsymbol{O}(\vec{\boldsymbol{r}}, t)|^2\end{aligned} \tag{13}$$

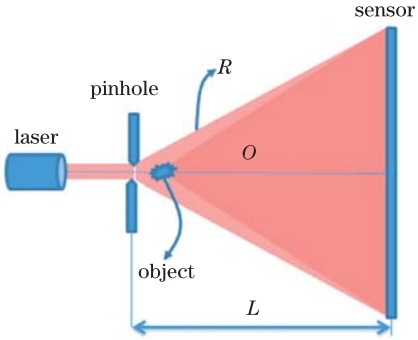

Fig. 3. (Color online) In-line DH with a spherical reference wave for recording of microscopic objects.

is the contrast enhanced hologram with a subtracted reference beam intensity after calibration measurement or by numerical processing; $r = \sqrt{x^2+y^2+L^2}$, and the vector $\vec{\xi}$ gives the coordinates of the object. The authors patented a fast algorithm for exact calculation of Eq. (12) and reported four-dimensional reconstruction of trajectories of moving micro-objects with wavelength resolution[43,44]. The twin-image has negligible impact being smeared in the reconstruction plane for the described geometry, especially for the used high numerical apertures at recording.

A single shot in-line holographic recording with a collimated reference beam was proposed in Refs. [45-48] under the name single-exposure on-line (SEOL) DH. The interference term written as

$$\begin{aligned}&\boldsymbol{O}(x,y)\,\boldsymbol{R}^{*}(x,y)+\boldsymbol{O}^{*}(x,y)\,\boldsymbol{R}(x,y)\\ =&a_{\mathrm{R}}\left[O_{\mathrm{h}}(x,y)+O_{\mathrm{h}}^{*}(x,y)\right],\end{aligned}\tag{14}$$

allows to estimate $O_{\mathrm{h}}(x,y)=a_{\mathrm{O}}(x,y)\exp\{i[\varphi_{\mathrm{O}}(x,y)-\varphi_{\mathrm{R}}(x,y)]\}$ from

$$O'_{\mathrm{h}}(x,y)=\left[I_{\mathrm{H}}(x,y)-a_{\mathrm{O}}^{2}(x,y)-a_{\mathrm{R}}^{2}(x,y)\right]/a_{\mathrm{R}},\tag{15}$$

where $|\boldsymbol{R}(x,y)|^2$ is obtained from a calibration measurement. The object beam intensity can be preliminary measured or removed by averaging. The Fresnel's transform of $O'_{\mathrm{h}}(x,y)$ reconstructs the object field with approximation due to the twin image term. In Ref. [48] the authors determined the conditions which guaranteed that the image reconstructed from $O'_{\mathrm{h}}(x,y)$ was close to the image, reconstructed from $O_{\mathrm{h}}(x,y)$, by using Wigner distribution formalism. Analysis in the phase space (spatial—spatial frequency domain) evaluates the cross-talk term after the inverse Fresnel transform of the conjugate term $O_{\mathrm{h}}^{*}(x,y)$ in $O'_{\mathrm{h}}(x,y)$. Analysis, made for DHM, shows that a real image of a lateral size L_{O} at magnification M_a is reconstructed correctly at spectral components which are higher than $M_aL_{\mathrm{O}}/2\lambda d$, where d is the recording distance. Comparable quality of reconstruction for a SEOL and PS DHM is reported.

The two-beam interference Eq. (1) logically leads to PS retrieval of the complex object field by means of multiple holograms capture. Acquisition of at least three fringe patterns by adding stepwise phase shifts $\phi_l, l = 1, 2, \cdots, n$ in $\boldsymbol{R}(x,y)$ results in non-ambiguous retrieval of $\boldsymbol{O}(x,y)$. Increasing the number of the phase shifts improves as a whole accuracy of the wavefront determination. The PS technique demodulates effectively fringe patterns with non-monotonous phase variation. The phase shifts can be introduced by using wave plates, a piezo-electric transducer mirror or an electro-optic modulator. For the phase step of $\pi/2$, $\boldsymbol{O}(x,y)$ is obtained from[49,50]

$$\begin{aligned}\boldsymbol{O}(x,y)=&\frac{1}{4\boldsymbol{R}^{*}}\{I_{\mathrm{H}}(x,y;0)-I_{\mathrm{H}}(x,y;\pi)\\ &+j\left[I_{\mathrm{H}}(x,y;\pi/2)-I_{\mathrm{H}}(x,y;3\pi/2)\right]\},\end{aligned}\tag{16}$$

for the four-step algorithm and from

$$\begin{aligned}O(x,y)=&\frac{1-j}{4R^{*}}\{I_{\mathrm{H}}(x,y;0)-I_{\mathrm{H}}(x,y;\pi/2)\\ &+j\left[I_{\mathrm{H}}(x,y;\pi/2)-I_{\mathrm{H}}(x,y;\pi)\right]\}\end{aligned}\tag{17}$$

for the three-step algorithm, where $I_{\mathrm{H}}(x,y;\phi_i)$ is the hologram recorded at the phase shift ϕ_i. Both zero-order and twin images are excluded from the reconstruction. Various aspects of image formation and quality are studied in Refs. [50-52] taking into account the discrete acquisition, bit depth limitations in hologram quantization, and color acquisition at three wavelengths.

Along with the carrier frequency approach the PS holography becomes the current state of the art technique in decoding phase information with a large scope of applications as DHM[50,53], encryption[54], optical diffraction tomography[55,56], shape and deformation measurement[57]. The PS approach with successive acquisition of digital holograms in time entails recording on a vibration-free optical table and renders impossible monitoring of dynamic events. Accuracy of the phase-shifts is also a crucial issue since any errors in their values inevitably result in occurrence of the twin image[58]. Object wave reconstruction with arbitrary unknown phase-steps from three or more fringe patterns is proposed and proved by simulation in Ref. [59].

A lot of efforts have been dedicated to developing an algorithm with acquisition of less than three patterns. Gabor and Goss in the 1960s were first to propose non-digital quadrature PS holography[60], whose experimental implementation, however, was rather complicated. It was further developed in Ref. [61,62] as two-reference wave version of the PS holography. A phase shift which is different from $l\pi$ where l is an integer is required. The results obtained with only two holograms recorded at $\pi/2$ shift in the reference beam proved the idea feasibility provided both reference and object beams intensities were separately measured. It is shown in Ref. [63] that the zero-order term can be removed by a calibration measurement of the reference wave. Quadrature PS holography method, proposed in Ref. [64], determines $\boldsymbol{O}(x,y)$ from

Table 1. Spatial-carrier Frequency Solutions

Solution	Complexity		Twin Image Removal	Pros	Cons
	Technical	*Numerical*			
Spatial Filtering in the Frequency Domain	Single Frame	Low	Complete	Real-time Capture	Decreased Bandwidth, Image Artifacts
Spatial PS	Single Frame	Low	Complete	Real-time Capture	Decreased Resolution
Non-linear Object Wave Retrieval	Single Frame	High	Complete	Real-time Capture, Larger Field of View	Constraints on the Object Complex Amplitude

the sum of four holograms recorded with four reference waves which are in quadrature with each other. Real-time two-step PS with two orthogonal polarizations introduced in the reference beam and detection by a CCD camera with checker boarded pixelated polarizers is verified in Ref. [65]. Effective solution for the real-time PS technique is spatial division of a single hologram into several holograms by inserting an array of 3×1 or 2×2 phase retarders[66,67] with phase-shifts which differ at $\pi/2$ in the reference wave. The array is imaged on the 2D photo-sensor; the size of the imaged array cells corresponds to the sensor's pixels size. The phase-shifted holograms are numerically generated from the recorded single-shot hologram using the pixels with the same phase-shift to form a new fringe pattern through keeping the positions of the extracted pixels and interpolating the intensity values in the surrounding pixels. For high phase retrieval accuracy the object surface variation is assumed comparatively small. The method is known under the name parallel PS holography. Its further improvement had been reported with an 2×1 array of retarders[67]. The intensity I_{R} is measured beforehand and $I_{\mathrm{R}} >> I_{\mathrm{O}}$ is assumed. A 262500-frames-per-second two-step parallel PS digital holography is reported in Ref. [68].

Interesting implementation of the single-shot PS technique is proposed in Ref. [69] by using a Talbot effect. A periodic diffractive optical element with a spatial period L_{DOH}, that consists of 2×2 cells with phase values, $l\pi/2, l = 0, 1, 2, 3$, is placed in a plane reference beam at a Talbot distance, $d_{\mathrm{T}} = 2L_{\mathrm{DOH}}^2/\lambda$, from the photo sensor. The photo sensor records the self-image of the structure encoded in the diffractive optical element without direct contact with it and without influencing the object beam. Talbot phenomenon is used again at reconstruction by multiplying the recorded multiplexed hologram with four binary masks to obtain the holograms with the phase shifts, $l\pi/2, l = 0, 1, 2, 3$, and propagating these holograms at a distance $d_{\mathrm{T}}/4$. An off-axis PS recording was used in Ref. [70] to reach sensitivity at the quantum level. The zero-order and the twin images are removed by spatial filtering whereas PS technique contributes to accuracy improvement. The goal is operation at extremely low signal level in order to perform nano-object imaging. Analysis of noises and aliases of the system is made in Ref. [71]. Spatial PS algorithm without a spatial carrier is proposed in Ref. [72]. Similarly to the other algorithms of this type, it implies constant background and contrast of the recorded fringe pattern in the vicinity of the point of interest. By expressing the phase of the object field as a Taylor's expansion, the Carre algorithm[73] is applied with a phase step which varies along the fringe pattern. This feature leads to variable measurement sensitivity and to occurrence of singularities at points with a zero phase gradient. The algorithm is stabilized by an iteration procedure. Elimination of the zero-order term by recording of two images and the twin image by recording of three or four images with phase-shifts produced by a liquid crystal phase modulator is proposed in Ref. [74]. However, the approach is a modified PS algorithm.

As in the previous section, Table 2 gives brief summary of the instrumental solutions to the twin image problem in in-line DH. It is clear that the temporal PS technique provides the best quality of the reconstructed image among the existing twin removal techniques. It can be applied to an arbitrary object. However the real-time capture is sacrificed. Nevertheless, the method can boast with a wide scope of applications. Parallel PS allows for fast acquisition rate at the expense of increased hardware complexity and slightly decreased spatial resolution. Single-frame in-line set-ups yield reconstructions contaminated to some degree by the twin image noise, so in this case the result is twin image reduction. Table 2 contains the same categories as Table 1 to alleviate comparison between off-line and in-line holographic systems.

5. In-line geometry—numerical elimination

Numerical approaches for twin image suppression in in-line DH can be categorized following different criteria as: i) iterative and non-iterative approaches, ii) diffraction-based and inverse problem solutions; iii) reconstruction of purely real or phase objects and of complex objects; iv) reconstruction of plane and volume objects, etc.. Most solutions are adopted from phase retrieval methods in optical metrology. Very frequently, they solve the twin image problem for a specific task or object. The general feature of the invented solutions is adoption of various simplifications.

Table 2. Instrumental Solutions for In-line Geometry

Solution	Complexity		Twin Image	Pros	Cons
	Technical	*Numerical*	Removal		
Spherical Reference Wave In-line Geometry	Single Frame; Calibration Measurement	High	Incomplete	Real-time Operation	Only Micro-objects
Temporal PS	Multiple frames, Phase Shifts Introduction	Low	Complete	Larger bandwidth	Vulnerable to Vibrations, Phase Shift Error
Parallel PS	Single-frame; Calibration Measurement; Pixelated Polarizers or Phase Retarders	Low	Complete	Real-time Operation	Decreased Bandwidth
SEOL DH	Single Frame, Calibration Measurement	Low	Incomplete	Real-time Operation	Constraints on the Object Complex Amplitude

For real plane objects transforming of the models (8) and (9) into[18,19]

$$I_{\mathrm{H}} - 1 = -2\tau * \Re\{h_z\}, \tag{18}$$

$$\Gamma - 1 = -\tau * (\delta + h_{2z}), \tag{19}$$

justifies a search for a deconvolution approach. The hologram and the reconstructed image can be considered as outputs of linear systems with transfer functions[18,19]

$$H_I(\nu_x, \nu_y) = 2\cos\frac{\lambda z}{4\pi}\left(\nu_x^2 + \nu_y^2\right), \tag{20}$$

$$H_\Gamma(\nu_x, \nu_y) = 1 + \exp\left\{-j\frac{\lambda z}{4\pi}\left(\nu_x^2 + \nu_y^2\right)\right\}, \tag{21}$$

respectively. One could expect that N data points in the hologram should provide reconstruction of N data points in the real object. However, the underlying twin image problem, which arises from the lack of phase information at the recording, expresses itself as occurrence of zeros of H_I and H_Γ along concentric circles in the Fourier domain. This entails looking for approximations to $1/H_I$ or $1/H_\Gamma$ in order to build inverse filters for deconvolution of the kernels in Eqs. (18) and (19). A truncated linear inverse filtering is proposed in Ref. [18] for processing of holograms of small objects described by a set of 2D opacity functions in particle imaging. The algorithm is derived for a single object plane, but it can work for a multiplanar distribution of particles if the separate diffraction planes are independent of each other. A proper series approximation to the inverse of the system singular transfer Eq. (20) is found that converges in the energy sense to the searched filter. The algorithm requires only a single fast Fourier transform pair. The authors comment that the algorithm is equivalent to computation of a series of holograms at distances$2^l z$, $l = 0, 1, 2, \cdots$ A purely absorptive thin object is considered in Ref. [75] at assumption of negligible scattering of the light wave inside it. It is shown that for a finite extent object the frequencies $\nu_x^2 + \nu_y^2 = l/\lambda z, l = 1, 2, 3, \cdots$ are not needed for its reconstruction. For the deconvolution of Eq. (19) the spectrum of the reconstructed image is multiplied in the frequency domain by a linear filter which is composed as $(H_\Gamma + \varepsilon)^{-1}$, where $\varepsilon = 10^{-2}$. The technique can be modified to work with a purely imaginery object. An iterative algorithm for subtraction of the intermodulation term is proposed. It is shown also that a complex object can be fully reconstructed if it is confined within a circle with a diameter less or equal to $\sqrt{0.186\lambda z}$. To apply the deconvolution technique to the hologram of a complex object, a non-iterative two intensities algorithm based on digital filtering is proposed in Ref. [76] under the constraints of weak scatterers and Fresnel approximation. The intensities, $I_{\mathrm{H}}^{1,2}$, in the two planes at distances z_1 and z_2 from the object yield the 2D functions $D_{1,2} = \exp(-jkz_{1,2})\left(I_{\mathrm{H}}^{1,2} - 1\right)$ which lead to[76]:

$$\begin{aligned} D_1 - D_2 * h_d =& \vartheta * \left[e^{-2jkz_1} h_{z_1} - e^{-2jkz_2} h_{z_2+d}\right] \\ =& \vartheta * \mathrm{H}, \end{aligned} \tag{22}$$

where $d = z_1 - z_2$. Different regularization schemes are tested to avoid the singularities of the inverse filter which is built to deconvolve H.

The close relation of the approaches based on inverse filtering of (18) and (19) to a class of iterative approaches in the spatial domain for recovery of images of 2D objects has been noted in Refs. [18,19]. Denis et al.[19] proposed a deconvolution point of view classification by showing that expansion of $1/H_\Gamma$ into a series as $1/(1+x) = 1 - x + \cdots + (-1)^l x^l$ is equivalent to generating a twin image from a distance $(2l+2)z$. Such a generation involves iterative reconstructions $\vartheta_{n+1}^* = \Gamma - \vartheta_n^* * h_{2z}$ at $\vartheta_0^* = \Gamma$. Iterative suppression of the twin image for complex 2D objects with a finite spatial support relies on removal of the in-focus image in the region of its support and iterative restoration of the out-of-focus image in the same region by going back and forth between the two reconstruction planes[77,78]. The recording geometry should ensure several times larger size of the region occupied by the out-of-focus image in comparison to the in-focus image. To make the task linear it is assumed that, under plane wave illumination, the dc term, I_{R}, dominates, so $I_{\mathrm{R}} >> I_{\mathrm{O}}$ is fulfilled everywhere in the hologram. The crucial issue for the algorithm is correct automatic evaluation of the object support from the reconstructed image, Γ. Different focus metrics and threshold approaches have been tested for reconstruction of real and phase objects[78–80]. This method works well for plane objects. It was further developed for automatic suppression of twin images for particles distributed in a 3D volume[19] by its coarse sampling with multiple planes. The redundancy of the Fresnel transform requires masking of the twin image of a given object in all planes. This is done by successive subtraction of contributions from the focused twin images of particles in all planes of the 3D volume from the complex amplitude in the hologram plane at each iteration.

In principle, the properties of the chirp Eq. (5) make possible reconstruction of a complex valued object by recording two holograms at different distances[81,82]. Solution of the twin-image problem inherent for the in-line geometry by optical subtraction of two holograms recorded at distances z and $2z$ from the object has been proposed practically at the dawn of holography in Ref. [83]. However, the idea proved to be of no use till the digital realization replaced its unpractical optical implementation[84]. Subtraction of the hologram intensity, I_{H}^{2z}, from the reconstructed image, $I_{\mathrm{H}}^{z} * h_z$, where the indices z and $2z$ correspond to distances between the hologram and the object, was studied by simulation for a small real-valued object in soft X-ray holography[81]. A simple non-iterative approach is proposed in Ref. [82] for reconstruction of weakly absorbing and weakly refracting objects by processing I_{H}^{z} and I_H^{2z}. The approach relies on the expansion of the exponent $\exp(i\varphi_0) \cong 1 + i\varphi_0$. The complex amplitude of the object beam is given as $O = (1-\vartheta)\exp(i\varphi_O) \approx 1 - \tilde{\vartheta}$, where $\tilde{\vartheta} = \vartheta - \iota\varphi_{\mathrm{O}}$. The amplitude and the phase are determined from $\vartheta = \frac{I_{\mathrm{H}}^{2z}+1}{2} - I_{\mathrm{H}}^{z} * Re(h_z)$ and $\varphi_{\mathrm{O}} \approx -i\left(1 - I_H^{2z} - \vartheta * h_z^* - \vartheta * h_z\right)\sum_{k=1}^{M} h_{(2k-1)z}$.

The reference beam is a unity amplitude plane wave. Another approach which relies on $I_{\mathrm{O}} << I_{\mathrm{R}}$ is proposed in Ref. [85] where two holograms, I_{H}^{z} and $I_{\mathrm{H}}^{z+\Delta z}$, are recorded. The approximation $\exp(-ikz)[a_{\mathrm{R}}+\boldsymbol{O}(x,y)] \approx a_{\mathrm{R}}\exp(-ikz)\exp(\boldsymbol{O}')$ is accepted with $\boldsymbol{O}' = \boldsymbol{O}/a_{\mathrm{R}}$ which for $a_{\mathrm{O}} \leqslant 0.1a_{\mathrm{R}}$ introduces error of 0.5%. By constructing the function $l_z = \log\left(I_{\mathrm{H}}^{z}/a_{\mathrm{R}}^{2}\right)$, one obtains the difference $F\{l_z\} - F\{l_{z+\Delta z}\}H_{\Delta z} = F\{\boldsymbol{O}\}_{z=0}H_z[1-H_{2\Delta z}]$ of its Fourier spectra in both measurement planes, where $H_z(\nu_x,\nu_y) = F\{h_z(x,y)\}$ is the known transfer function of free propagation and $F\{\boldsymbol{O}\}_{z=0}$ is the angular spectrum of the object at $z=0$. The algorithm was verified by simulation for a 2D object. It is applicable for real-time reconstruction if two photo sensors are used. This algorithm is called optical-path-length-shifting DH in Ref. [86] where a phase-retardation array consisting of 2×1 pixels generates two-step optical-path-length difference or two-step phase shift for both the object wave and the reference wave. Thus real-time operation is achieved with a single photo sensor. The phase shift between the two types of pixels can take any value different from $0.5(l+1)\lambda$ where l is an integer. Reconstruction of discrete objects of high spatial frequency from a single in-line hologram is made in Ref. [87] by building a real image of an object from the hologram points which are far away from the optical axis and correspond to off-axis geometry. The authors even introduced the name "off-axis reconstruction" of in-line hologram.

As we have stated above, twin image elimination by numerical means is related to phase retrieval problems from intensity data. Once the phase is retrieved, one reconstructs the object wave with the known amplitude. However, the task is ill-posed in the case of a single hologram because the $2N$ parameters which give the complex amplitude of the object field should be retrieved from N parameters in the hologram plane[12]. A Gerchberg-Saxton algorithm[88] and related algorithms have been initially developed for phase retrieval from two intensity measurements[89]. For the non-periodic objects this is done through iterative Fourier transformation back and forth between the object and Fourier domains and applying the amplitude data in both domains. These algorithms underwent generalization by applying partial a priori constraints in both domains in order to solve a large class of problems. Thus phase retrieval from a single intensity measurement becomes possible. The developed by Fienup error-reduction approach and its faster converging modification under the name "input-output" algorithm[90] recover a real non-negative object with a loose support constraint from the modulus of its Fourier transform. Reconstruction of a complex-valued object from this modulus was proven possible in the case of a tight support which coincides with the true boundaries of the object[91]. It is practically possible to achieve unique solution for the 2D sampled objects of finite support. If the sampled object amplitude is non-zero within a mask with a polygon shape without parallel sides and zero outside, phase retrieval from the autocorrelation function of the object is unique[92]. Phase retrieval from a correctly sampled modulus of Fourier transforms is underdetermined by a factor of 2 for 1D, 2D, and 3D objects[93]. To make it possible, one should decrease the number of unknowns, e.g., by using known-valued pixels. Effective way to increase their number is to oversample the modulus of the Fourier transform. Simulation in Ref. [93] proves the accurate phase retrieval from the oversampled modulus of the Fourier transforms of 2D and 3D complex-valued objects by using positivity constraints on the imaginary part of the objects and loose supports. The requirement for oversampling is much less than 4 for 2D and 8 for 3D objects.

In in-line Fresnel DH the hologram and its transform domain are not related directly by a Fourier transform. In addition, twin images are trivial characteristics of the phase problem. However, by forming an iterative loop between the hologram and the reconstruction plane, it is possible to eliminate the twin image by an error-reduction algorithm from a single intensity measurement under the constraint of a real object in the object domain[94]. Iterative approach based on propagation back and forth between the hologram and the object plane is proposed in Ref. [95] where the propagation operator (Eq. (12)) is used to cope with any illumination geometry. A complex-valued object of arbitrary size and shape is considered without the requirement for tight support. By recording of the reference wave beforehand, the hologram is normalized. Domination of the reference wave over the object wave is not mandatory. The hologram plane constraint is the known magnitude of the normalized hologram whereas in the object plane it is an absorptive object. Assumption of single scattering within the object restricts application of the method to in practice 2D objects. A Gerchberg-Saxton algorithm which self-adapts to the object finite extent and shape is applied in Ref. [12] to holograms of ice crystals. The algorithm assumes a complex-valued object in a single plane without objects in the other planes and diffraction fields coming from them. The background occupies m points in the object plane, which means that $2m$ parameters are constant there. At $m > N/2$, the number of unknown parameters in the object plane is smaller than in the hologram plane which is the basis for the algorithm. The object plane constraint is uniformity of the object field outside the object whereas the hologram plane constraint is the hologram amplitude. For faster algorithm convergence a mask is adjusted during the iteration process. Image reconstruction with a Yang-Gu algorithm in in-line DH is proposed in Ref. [96] and verified for a real object. The Yang-Gu algorithm is an enhanced version of the conventional Gerchberg-Saxton algorithm and can be applied for an optical system with a diffraction loss or for non-paraxial systems—the case, in which the reconstruction integral operator, $\boldsymbol{G}$, is a non-unitary operator, $\boldsymbol{G}\boldsymbol{G}^{*} = \boldsymbol{A} \neq \boldsymbol{I}$, where $\boldsymbol{A}$ is a Hermitian operator and $\boldsymbol{I}$ is an identity transform[97,98]. The algorithm is based on minimization of the square of the ℓ^2 norm $||\Gamma - \boldsymbol{G}I_{\mathrm{H}}||^2$. It shows much less sensitivity to the recording distance whose increasing enhances the non-unitary character of the transform between the hologram and the reconstruction plane. The study in Ref. [96] shows that both Yang-Gu and Gerchberg-Saxton algorithms require at least 8-bit encoded digital holograms and exhibits the same vulnerability to the additive noise.

Approaches based on the data statistics and a physical model of the optical system have been analyzed in Ref.

[99,100]. Statistical image reconstruction is formulated as an ill-posed inverse problem in which the primary image is a complex object field. The challenges are reconstruction of complex-valued signals from real intensity data and the highly random phase of the scattered fields in holography of diffuse objects. The solution is sought through regularization methods. The signal Y_i at the i-th pixel of the photosensor is modeled as a random quantity with a mean value equal to I_i+b, where I_i is the intensity of the hologram and b is the noise mean value. The reconstructed image is found as a minimizer of a cost function through an iterative process. In Ref. [100] this is done through formal extension of half-quadratic regularization techniques to complex-valued, random-phase fields and a penalized-likelihood estimation with a Poisson statistical model of the data. The true object field is represented as a linear combination of basic functions. The model is developed for incoherent holography to avoid the speckle which rather complicates the noise model. Optimization problem is simplified by finding a "surrogate function" which lies above the original cost function at each iteration. Reconstruction schemes with one or two holograms are proved by simulations. Inverse-problem approach as a contrary to the conventional Fresnel approach was applied for fine localization of particles and improvement of the transverse field of view in in-line DH for the diluted media[101,102]. A sparsity hypothesis is valid in this case, and the hologram is modeled as a linear sum of the diffraction inputs from all particles[103]. The size and 3D coordinates of the particles are found iteratively by solving a minimization problem. In Ref. [101], after coarse focusing by Fresnel reconstruction for initial guess of particles positions, fine localization of each particle is performed through a nonlinear fit of a hologram model to the hologram image by minimizing the weighted least squares penalty. After that this particle contribution to the hologram is subtracted. The iterations continue till no particle remains non-detected. Reconstruction through solving global optimization problem makes this approach insensitive to the twin-image problem. It is further improved in Ref. [104] for reconstruction of particles positions outside the camera field of view. The same inverse problem in Ref. [102] is solved by minimization of a ℓ^1 norm for reconstructing more general objects than particles provided they obey the sparsity criterium.

Real-time reconstruction of the complex amplitude is proposed in Ref. [105] by simultaneous recording of the hologram and the 3D object intensity distribution using two cameras. Processing of these two images provides the amplitude and the object phase absolute value. The phase sign is obtained by an iterative algorithm which cuts the twin image from the plane of its focus and propagates the resulting complex amplitude to the plane of the real image. The process stops where there is no change in the sign of the phase in the hologram plane. Separation of the terms $\boldsymbol{RR}^*$, $\boldsymbol{OO}^*$ and $\boldsymbol{OR}^* + \boldsymbol{O}^*\boldsymbol{R} = a_{\mathrm{R}}a_{\mathrm{O}}\cos(\varphi_{\mathrm{O}} - \varphi_{\mathrm{R}})$ by an independent component analysis is proposed in Ref. [106]. A linear combination of these terms is formed from three holograms as a sum $\alpha_l a_{\mathrm{R}}\cos(\beta_l\varphi_{\mathrm{R}}) + \delta_l a_{\mathrm{O}}\cos(\gamma_l\varphi_{\mathrm{O}})$ where α_l, β_l, δ_l, γ_l, $l = 1, 2, 3$ are taken as random numbers which vary a little in the reference and object beams due to the random nature of the recording process. Separation of the real and twin image regions by a blind separation matrix and suppression of the twin image by the segmentation mask is proposed in Ref. [107]. The approach gives better result than the overlapping block variance and manual-based schemes for outlining the image regions.

Table 3 summarizes the properties of numerical solutions to the twin image problem in in-line geometry. Development of such approaches is dedicated practically entirely to reconstruction from a single in-line hologram to make possible real-time capture. However, till now, the twin image has been removed completely only for reconstruction of specific objects, e.g., plane objects, weakly scattering objects, objects with a tight support.

6. Elimination of the zero-order

The zero-order term can be eliminated by high-pass filtering of the hologram. Suppression of the background by averaged intensity subtraction[108] is reasonable only for uniform intensity distributions. A simple method for zero-order reduction and contrast enhancement in off-axis holography is developed in Ref. [109] through

Table 3. Numerical Solutions for In-line Geometry

Solution	Complexity		Twin Image Removal	Pros	Cons
	Technical	*Numerical*			
Deconvolution Approach	Single Frame	Low	Plane; Purely Real or Phase	Diffraction- Based, Non-iterative;	Incomplete
	Two Frames	Low	Plane; Complex		
In-focus Image Removal	Single Frame	High	Complex, Finite Support, Sparse Objects in 3D Volume	Diffraction-based, Iterative; Focus Metrics, Threshold Approaches	Incomplete
Hologram Capture at Different Distances	Two Frames	Low	Purely Real or Phase, Complex	Non-iterative	Incomplete
Phase Retrieval	Single Frame	High	Purely Real, Complex, 3D Volume	Iterative, Constraints	Complete for Specific Objects
	Two Frames			Iterative	
Inverse Problem Approach	Single Frame	High	Iterative, Constraints	Non-diffraction Based	Complete for Specific Objects

computing the Laplacian of the hologram and its further Fresnel reconstruction. Numerical elimination of the zero-order image from a single digital hologram is made in Ref. [110] by calculating approximately $I_{\mathrm{O}}(x,y)$ from the intensities $I_{\mathrm{H}}(x,y)$ and $I_{\mathrm{R}}(x,y)$ at known illumination geometry. The advantage is applicability to non-uniform distribution of the object wave. Analysis of quality of the zero-order suppression and deterioration of image reconstruction due to approximate intensity calculation[110] predicts reasonable results only at an intensity ratio $I_{\mathrm{R}}/I_{\mathrm{O}}$ from 7.90 up to 47.2. The authors comment that such a ratio does not provide best visibility of fringes. Real-time zero-order term elimination is done in Ref. [111] by subtraction of two subsequently recorded holograms with a stochastic change of the speckle introduced by stimulating vibrations of the optical table. The experiments made for a quasi Fourier off-axis DH proved successful elimination at a capture rate of 16 frames/s.

Zero-order suppression by non-linear filtering in off-axis recording geometry at partial overlapping of the zero-order and twin images spectra in the frequency domain is verified both by theory and experiment in Refs. [112–113]. Two requirements should be fulfilled: i)$I_{\mathrm{R}} > I_{\mathrm{O}}$; ii) the twin images spectra do not overlap, i.e. the object beam spectrum occupies one quadrant in the frequency domain. In addition, the reference wave is a plane wave and its intensity is determined from a calibration measurement. The complex amplitude of the object wave is determined from the cepstrum of the hologram, $c = F\{\log|1+\boldsymbol{O}/\boldsymbol{R}|^2\}$ normalized to I_{R}[113]:

$$O = R\Big[\exp\Big(F^{-1}\Big[F\Big\{\log\Big|1+\frac{\boldsymbol{O}}{\boldsymbol{R}}\Big|^2\Big\} \cdot \mathbf{1}_{[0,\infty)\times[0,\infty)}\Big]\Big) - 1\Big], \tag{23}$$

where $\mathbf{1}_{[0,\infty)\times[0,\infty)}$ is an indicator window function to select the proper quadrant. The main advantage is increase in the allowed bandwidth of the object spectrum. For an object with a discrete circular spectral support with radius, that is recorded in a square hologram with N pixels, the classical spatial filtering method sets a limitation on the maximal value of the object spectral support as $a^{\mathrm{SF}} = \sqrt{N}/\big(2+3\sqrt{2}\big)$, whereas the non-linear filtering provides $a^{\mathrm{NF}} = \sqrt{N}/4$[113].

A method for zero-order suppression which relies on periodicity of images in DH and space-shifting property of the Fourier transform is proposed in Ref. [114]. According to the authors, the image and the dc noise have different reconstruction periods related to the different CCD sampling periods for the interference and the dc terms of the hologram. However, there is no explanation how they succeed to sample separately both terms.

7. Conclusion

Elimination of the zero-order and twin image terms in numerical reconstructions from holographic fringe patterns is a key requirement for quality improvement in DH. Introduction of a spatial carrier in the recorded digital hologram is a straightforward solution to this task at a cost of decreasing the allowed bandwidth of object wave. If the spectra of the twin images are separated in the spatial frequency domain, relevant information about the object complex amplitude is retrieved by applying a proper window function in this domain. Otherwise, spatial PS in different modifications and wavelet transform proved to retrieve successfully the object wave from a single hologram with a spatial carrier. The twin image removal problem in in-line DH has been effectively attacked by instrumental means. Among the approbated techniques, the temporal PS is the most reliable solution but requires capture of multiple holograms. Reducing the required number of holograms continues to attract a lot of research efforts together with elaboration of single hologram approaches as a point source DHM or introduction of calibration measurements. Complexity of the twin image problem predetermined development of numerical solutions dedicated to a specific task or type of objects. Specificity of the task allows for derivation of constraints which make possible retrieval of the object wave from the intensity data. The existing solutions include iterative and non-iterative approaches, diffraction-based and inverse problem solutions; reconstruction of purely real or phase objects and of complex objects, reconstruction of plane and volume objects. Elimination only of the zero-order is also frequently addressed topic which is usually solved by means of additional calibration measurements. Recently, some more sophisticated techniques as non-linear filtering in the frequency domain have been proposed. In summary, complete removal of the unwanted zero- and twin images in reconstructions from digital holograms of arbitrary 3D objects is achieved by increasing the number of the recorded holograms or by decreasing the spatial resolution or useful bandwidth for the case of a single hologram. Removal by numerical means, especially in case of a single hologram, provides good results only under task or object oriented constraints and remains a challenging research field.

8. Acknowledgement

This work was supported by the IT R&D program of MSIP (Fundamental technology development for digital holographic contents).

References

1. D. Gabor, Nature **161,** 777 (1948).
2. E. Leith and J. Upatnieks, J. Opt. Soc. Am. **52,** 1123 (1962).
3. U. Schnars, J. Opt. Soc. Am. A **11,** 2011 (1994).
4. U. Schnars and W. P. O. Jüptner, Appl. Opt. **33,** 179 (1994).
5. U. Schnars and W. P. O. Jüptner, Meas. Sci. Technol. **13,** R85 (2002).
6. U. Schnars and W. Jueptner, *Digital Holography* (Springer-Verlag, 2005).
7. F. Dubois, N. Callens, C. Yourassowsky, M. Hoyos, P. Kurowski, and O. Monnom, Appl. Opt. **45,** 864 (2006).
8. J. M. Desse, P. Picart, and P. Tankam, Opt. Express **16,** 5471 (2008).
9. Y L. Denis, C. Fournier, T. Fournel, C. Ducottet, and D.Jeulin, Appl. Opt. **45,** 944 (2006).
10. L. De Caro, C. Giannini, D. Pelliccia, C. Mocuta, T. H. Metzger, A. Guagliardi, A. Cedola, I. Burkeeva, and S. Lagomarsino, Phys. Rev. B **77,** 081408(R) (2008).

11. P. Korecki, G. Materlik, and J. Korecki, Phys. Rev. Lett. **86,** 1534 (2001).
12. S. Raupach, Appl. Opt. **48,** 287 (2009).
13. Y L. Xu, J. Miao, and A. Asundi, Opt. Eng. **39,** 3214 (2000).
14. S. Grilli, P. Ferraro, S. De Nicola, A. Finizio, and G. Pierattini, R. Meucci, Opt. Express **9,** 294 (2001).
15. L. Xu, X. Peng, Z. Guo, J. Mia, and A. Asundi, Opt. Express **13,** 2444 (2005).
16. Y M. K. Kim, *Digital Holographic Microscopy: Principals, Techniques, and Applications* (Springer, 2011).
17. P. Picart and J. Leval, J. Opt. Soc. Am. A **25,** 1744 (2008).
18. L. Onural and P. Scott, Opt. Eng. **26,** 1124 (1987).
19. L. Denis, C. Fournier, T. Fournel, and C. Ducottet, Meas. Sci. Technol. **19,** 074004 (2008).
20. E. Cuche, P. Marquet, and C. Depeursinge, Appl. Opt. **39,** 4070 (2000).
21. E. Cuche, P. Marquet, and C. Depeursinge, Appl. Opt. **38,** 6994 (1999).
22. Y J. Kühn, F. Charrière, T. Colomb, E. Cuche, F. Montfort, Y. Emery, P. Marquet, and C. Depeursinge, Meas. Sci. Technol. **19,** 074007 (2008).
23. P. Massatsch, F. Charrire, E. Cuche, P. Marquet, and C. D. Depeursinge, Appl. Opt. **44,** 1806 (2005).
24. F. Charrière, A. Marian, F. Montfort, J. Kuehn, T. Colomb, E. Cuche, P. Marquet, and C. Depeursinge, Opt. Lett. **31,** 178 (2006).
25. Y. Pu and H. Meng, J. Opt. Soc. Am. A **21,** 1221 (2004).
26. J. H. Massig, Opt. Lett. **27,** 2179 (2002).
27. Y Z. Ansari, Y. Gu, M. Tziraki, R. Jones, P. M. W. French, D. Nolte, and M. Melloch, Opt. Lett. **26,** 334 (2001).
28. Q. Lü, B. Ge, J. Jiang, Y. Zhang, Proc. SPIE **5636,** 254 (2005).
29. E. Garbusi, C. Pruss, and W. Osten, Appl. Opt. **47,** 2046 (2008).
30. M. Kujawinska and J. Wójciak, Proc. SPIE **1508,** 61 (1991).
31. Y M. Pirga and M. Kujawinska, Opt. Eng. **34,** 2459 (1995).
32. H. Guo, Q. Yang, and M. Chen, Appl. Opt. **46,** 1057 (2007).
33. J. D. Tobiason and K. W. Atherton, "Interferometer using integrated imaging array and high-density polarizer array" US Patent 6850329 B2 (2005).
34. J. E. Millerd, N. J. Brock, J. B. Hayes, M. B. North-Morris, B. T. Kimbrough, and J. C. Wyant, Proc. SPIE **5531,** 304 (2004).
35. Y B. T. Kimbrough, Appl. Opt. **45,** 4554 (2006).
36. T. Tahara, Y. Shimozato, Y. Awatsuji, K. Nishio, S.Ura, O. Matoba, and T. Kubota, Opt. Lett. **37,** 148 (2012).
37. M. Liebling, T. Blu, and M. Unser, J. Opt. Soc. Am. A **21,** 367 (2004).
38. D. Carl, B. Kemper, G. Wernicke, and G. von Bally, Appl. Opt. **43,** 6536 (2004).
39. B. Kemper and G. von Bally, Appl. Opt. **47,** A52 (2008).
40. M. Liebling, T. Blu, and M. Unser, IEEE Trans. Image Proc. **12,** 29 (2002).
41. J. Zhong and J. Weng, Appl. Opt. **43,** 4993 (2004).
42. J.Weng, J. Zhong, and C. Hu, Opt. Express **16,** 21971 (2008).
43. J. Garcia-Sucerquia, W. Xu, S. K. Jericho, M. H. Jericho, P. Klages, H. J. Kreuzer, Appl. Opt. **45,** 836 (2006).
44. M. H. Jericho and H. J. Kreuzer, in *Coherent Light Microscopy: Imaging and Quantitative Phase Analysis* P. Ferraro, A. Wax, Z. Zalevsky, (eds.) (Springer-Verlag Berlin, Heidelberg, 2011) chap. 1.
45. D. Kim and B. Javidi, Opt. Express **12,** 5539 (2004).
46. B. Javidi and D. Kim, Opt. Lett. **30,** 236 (2005).
47. B. Javidi, I. Moon, S. Yeom, and E. Carapezza, Opt. Express **13,** 4492 (2005).
48. A. Stern and B. Javidi, J. Opt. Soc. Am. A **24,** 163 (2007).
49. Yamaguchi and T. Zhang, Opt. Lett. **22,** 1268 (1997).
50. Yamaguchi, J. Kato, S. Ohta, and J. Mizuno, Appl. Opt. **40,** 6177 (2001).
51. Yamaguchi, T. Matsumura, and J.-I. Kato, Opt. Lett. **27,** 1108 (2002).
52. G. A. Mills and I. Yamaguchi, Appl. Opt. **44,** 1216 (2005).
53. T. Tahara, K. Ito, T. Kakue, M. Fujii, Y. Shimozato, Y. Awatsuji, K. Nishio, S. Ura, T. Kubota, and O. Matoba, Biomed. Opt. Express **1,** 610 (2010).
54. S. Lai and M. A. Neifeld, Opt. Commun. **178,** 283 (2000).
55. A. Devaney and J. Cheng, Meas. Sci. Technol. **19,** 085505 (2008).
56. Y. Sung, W. Choi, C. Fang-Yen, K. Badizadegan, R. R. Dasari, and M. S. Feld, Opt. Express **17,** 266 (2009).
57. I. Yamaguchi, in *Proceedings of Digital Holography and Three-Dimensional Imaging* **DWA,** DMA1 (2009).
58. J. Hahn, H. Kim, S.-W. Cho, and B. Lee, Appl. Opt. **47,** 4068 (2008).
59. L. Cai, Q. Liu, and X. Yang, Opt. Lett. **28,** 1808 (2003).
60. D. Gabor and W. Goss, J. Opt. Soc. Am. **56,** 849 (1966).
61. P. Guo and A. Devaney, Opt. Lett. **29,** 857 (2004).
62. Y. Wang, Y. Zhen, H. Zhang, and Y. Zhang, Chin. Opt. Lett. **2,** 141 (2004).
63. J.-P. Liu and T.-C. Poon, Opt. Lett. **34,** 250 (2009).
64. S. Lai, B. King, and M. Neifeld, Optics Commun. **173,** 155 (2000).
65. T. Nomura, S. Murata, E. Nitanai, and T. Numata, Appl. Opt. **45,** 4873 (2006).
66. T. Nomura, S. Murata, E. Nitanai, and T. Numata, Appl. Opt. **45,** 4873 (2006).
67. Y. Awatsuji, T. Tahara, A. Kaneko, T. Koyama, K. Nishio, S. Ura, T. Kubota, and O. Matoba, Appl. Opt. **47,** D183 (2008).
68. T. Kakue, M. Fujii, Y. Shimozato, T. Tahara, Y. Awatsuji, K. Nishio, S. Ura, T. Kubota, and O. Matoba, in *Proceedings of Digital Holography and Three-Dimensional Imaging* **DWC,** DWC25 (2011).
69. Siemion, M. Sypek, M. Makowski, J. Suszek, A. Siemion, D. Wojnowski, and A. Kolodziejczyk, Opt. Eng. **49,** 055802 (2010).
70. M. Gross and M. Atlan, Opt. Lett. **32,** 909 (2007).
71. M. Gross, M. Atlan, and E. Absil, Appl. Opt. **47,** 1757 (2008).
72. E. Garbusi, C. Pruss, and W. Osten, Appl. Opt. **47,** 2046 (2008).
73. P. Carré, Metrologia **2,** 13 (1966).
74. Y. Takaki, H. Kawai, and H. Ohzu, Appl. Opt. **38,** 4990 (1999).
75. K.Nugent, Opt. Commun. **78,** 293 (1990).
76. M. Maleki and A. Devaney, Opt. Eng. **33,** 3243 (1994).
77. G. Koren, D. Joyeux, and F. Polack, Opt. Lett. **16,** 1979 (1991).

78. G. Koren, F. Polack, and D.Joyeux, J. Opt. Soc. Am. A **10,** 423 (1993).
79. McElhinney, J. McDonald, A. Castro, Y. Frauel, B. Javidi, and T. Naughton, Opt. Lett. **32,** 1129 (2007).
80. McElhinney, B. Hennelly, and T. Naughton, J. Phys.: Conf. Ser. **139,** 012014 (2008).
81. T. Xiao, H. Xu, Y. Zhang, J. Chen, and Z. Xu, J. Mod. Opt. **45,** 343 (1998).
82. Y. Zhang, G. Pedrini, W. Osten, and H. J. Tiziani, Appl. Opt. **42,** 6452 (2003).
83. W. Bragg and G. Rogers, Nature **167,** 190 (1951).
84. L. Rogers, Opt. Lett. **19,** 67 (1994).
85. Y. Zhang, G. Pedrini, W. Osten, and H. Tiziani, Opt. Lett. **29,** 1787 (2004).
86. Y. Awatsuji, T. Koyama, T. Tahara, K. Ito, Y. Shimozato, A. Kaneko, K. Nishio, S. Ura, T. Kubota, and O. Matoba, Appl. Opt. **48,** H160 (2009).
87. S. Lai, B. Kemper, and G. von Bally, Opt. Commun. **169,** 37 (1999).
88. R. W. Gerchberg and W. O. Saxton, Optik **35,** 237 (1972).
89. J. Fienup, Appl. Opt. **21,** 2758 (1982).
90. J. R. Fienup, Opt. Lett. **3,** 27 (1978).
91. J. R. Fienup, J. Opt. Soc. Am. A **4,** 118 (1987).
92. T. R. Crimmins, J. Opt. Soc. Am. A **4,** 124 (1987).
93. J. Miao, D. Sayre, and H. N. Chapman, J. Opt. Soc. Am. A **15,** 1662 (1998).
94. G. Liu, and P. Scott, J. Opt. Soc. Am. A **4,** 159 (1987).
95. T. Latychevskaia and H. W. Fink, Phys. Rev. Lett. **98,** 233901 (2007).
96. Y. Zhang and X. Zhang, Opt. Express **11,** 572 (2003).
97. G. Yang and B. Gu, Acta Phys. Sin. (in Chinese) **30,** 410 (1981).
98. G. Z. Yang, B. Z. Dong, B. Y. Gu, J. Zhuang, and O. K. Ersoy, Appl. Opt. **33,** 209 (1994).
99. M. Cetin, W. C. Karl, and A. S. Willsky, in *Proceedings of the IEEE International Conference on Image Processing* 481 (2002).
100. S. Sotthivirat and J. Fessler, J. Opt. Soc. Am. A **21,** 737 (2004).
101. F. Soulez, L. Denis, C. Fournier, É. Thiébaut, and C. Goepfert, J. Opt. Soc. Am. A **24,** 1164 (2007).
102. L. Denis, D. Lorenz, É. Thiébaut, C. Fournier, and D. Trede, Opt. Lett. **34,** 3475 (2009).
103. J. Gire, L. Denis, C. Fournier, É. Thiébaut, F. Soulez, and C. Ducottet, Meas. Sci. Technol. **19,** 074005 (2008).
104. F. Soulez, L. Denis, É. Thiébaut, C. Fournier, and C. Goepfert, J. Opt. Soc. Am. A **24,** 3708 (2007).
105. T. Nakamura, K. Nitta, and O. Matoba, Appl. Opt. **46,** 6849 (2007).
106. X. Chai, C. Zhou, Z. Feng, Y. Wang, and Y. Zuo, Chin. Opt. Lett. **4,** 11 (2006).
107. Cho, B. Choi, H. Kang, and S. Lee, Opt. Express **20,** 22454 (2012).
108. T. Kreis and W. Jüptner, Opt. Eng. **36,** 2357 (1997).
109. C. Liu, Y. Li, X. Cheng, Z. Liu, F. Bo, and J. Zhu, Opt. Eng. **41,** 2434 (2002).
110. J.-P. Liu, T.-C. Poon, and T.-H. Yang, Opt. Eng. **50,** 091309 (2011).
111. N. Demoli, J. Mestrović, and I. Sović, Appl. Opt. **42,** 798 (2003).
112. Y N. Pavillon, C. S. Seelamantula, J. Kühn, M. Unser, and C. Depeursinge, Appl. Opt. **48,** H186 (2009).
113. C. Seelamantula, N. Pavillon, C. Depeursinge, and M. Unser, J. Opt. Soc. Am. A **28,** 983 (2011).
114. J. Wu, M.-F. Lu, Y. Dong, M. Zheng, M. Huang, and Y. Wu, Appl. Opt. **50,** H56 (2011).